This article has been accepted for publication in a future issue of this journal, but has not been fully edited. Content may change prior to final publication. Citation information: DOI 10.1109/TIA.2017.2787994, IEEE Transactions on Industry Applications

Model Predictive Control based Field-weakening Strategy for Traction EV used Induction Motor

Jianyong Su, *Member, IEEE*, Rui Gao, *Student Member IEEE* and Iqbal Husain, *Fellow, IEEE*

***Abstract*—The field-weakening scheme is generally adopted for traction motors to achieve a wider speed range where the common proportional and integration (PI) compensator is needed to regulate the flux-producing current. However, the regulator performance deteriorates due to the dc-link voltage disturbances and motor parameter nonlinearities in the different speed regions. To solve this issue, a model predictive control (MPC) based field-weakening algorithm is proposed for a traction Electric Vehicle (EV) using a low-voltage induction motor (IM). The augmented prediction state relationship between stator voltage and flux-producing current is established for motor current control. The steady-state error can be eliminated with an integrator embedded within the augmented equation. The overall closed-loop control is presented where the system eigenvalues are adjusted in real time for various speed regions, and accordingly the controller performance can be evaluated with the amplitude of the eigenvalues. Moreover, the weight coefficient in the cost function can be adjusted corresponding to speed variation for guaranteed motor control performance. The simulation and experimental results are provided to verify the proposed MPC based field-weakening algorithm.**

***Index Terms*—Field-weakening control, model predictive control (MPC), indirect field oriented control (IFOC), induction machine, electric vehicle.**

I. Introduction

With the growing interest in EVs and HEVs in the recent decades, significant effort is devoted for the development of efficient, reliable, and economical ac drives for such applications [1]. The traction drive system is required to work in a harsh and confined environment where the lasting full load conditions are possible [2], [3].

Both induction motors (IMs) and permanent magnet synchronous motors (PMSMs) are candidates for EV/HEVs [4], [5], where the motors need to operate over a wide speed range. The constant torque capability below the base speed and constant power capability over the base speed are two critical requirements for such applications where several times of the base speed might be required for eliminating the gear shifting in these vehicles [6], [7].

Electric forklift is a typical traction vehicle where two types of motors are used: one is for lifting pump, and the other is for traction drive. The low voltage induction machine is typically selected as the traction motor considering its advantages of cost, reliability, ruggedness and low maintenance compared with the PMSM [4], [8]. Since the pump motor control is easier compared with the traction one, this paper studies the latter one and investigates its control strategy in the field-weakening region which is typically 2 to 3 times of the base speed [9]. Electric forklift is a little different from the general EV. The maximum speed and accelerated speed should be limited at same time. The forklift should be still controlled when the accelerator pedal is released. The forklift speed is expected to follows the signal of accelerator pedal. Usually, the speed loop control is adopted in electric forklift.

One of the concerns for this region is the DC-link voltage fluctuations which may disrupt the control system [10], [11]. Typical electric forklifts utilize batteries as the supply, and the flux-producing current is inversely proportional to the rated one when the motor has to operate beyond the rated speed. This method is simple but is not suitable for EV with large DC-link voltage variation. Another solution is that the current reference is calculated based on IM parameters or updated with lookup tables, which relies on a good knowledge of motor parameters and the actual DC-link voltage values [12], [13]. However, these parameters are usually not constant due to the variation of temperature and magnetic hysteresis which makes such method inaccurate.

Others solve the motor parameter variation issue by adding extra voltage loop based on the PI regulator, with the output setting as the flux-producing current reference [14], [15]. However, when the required voltage value is larger than the available one, the speed tracking cannot be maintained due to insufficient DC-link voltage which limits the flux-producing current. However, the flux component is expected to be as large as possible such that a higher electromagnetic torque can be achieved [16]-[19]. However, possible issues with these types of methods are that only the *q*-axis voltage is considered and *d*-axis voltage is generally neglected in the PI regulator analysis. But the feedback of PI regulator is indeed a complex voltage composed of both *d*- and *q*-axis voltage components. Such simplification could lead to undesired flux-producing current oscillations. Meanwhile, the open-loop gain changes as the motor speed varies considering the angular speed involvement of the voltage equation. The parameter tuning further worsens the system performance and can cause stability issues [13]. The two aspects make it difficult to tune the voltage-loop PI parameters, and practically, this usually needs to be implemented based on a trial and error method [7].

There are three objectives for the field-weakening control of the traction IM. First, static errors should be eliminated when

Jianyong Su is with the School of Electrical Engineering and Automation, Harbin Institute of Technology, Harbin 150001,China (e-mail: sujianyong@hit.edu.cn).

Rui Gao and Iqbal Husain are with the Department of Electrical and Computer Engineering, North Carolina State University, Raleigh, NC27606, USA (e-mail:rgao@ncsu.edu; ihusain2@ncsu.edu).

This article has been accepted for publication in a future issue of this journal, but has not been fully edited. Content may change prior to final publication. Citation information: DOI 10.1109/TIA.2017.2787994, IEEE Transactions on Industry Applications

the condition changes due to motor parameter variation, the DC-link voltage level, the motor speed, etc. [6], [20]. Second, in the process of acceleration or deceleration, the flux-producing current needs to response promptly to ensure speed tracking ability. For traction EV, the changing rate of the speed reference is not as high as in other applications. The torque-producing current is tracked well and the calculated voltage from current regulators is almost equal to the required voltage. The tracking controller must have good response to speed changes [21]. Third, at the acceleration/deceleration transient stage, the calculated voltage reference tends to suffer severe oscillations caused by the drastic changing rate of *q*-axis current. In the transient process, the amplitude of the complex voltage is bigger than the required one, which distorts the flux-producing current reference. Therefore, the regulator is expected to be less sensitive to the variation of feedback voltage. Neither the second nor the third requirement be satisfied at the same time. The balance between them is the key during the parameter tuning process.

Model predictive control is an optimal control technology which is regarded as one of the most effective control strategies in process industries [22], [23]. In the last few years, MPC techniques are getting significant attention for the power electronics and electric drives applications [24]-[26]. Compared with the traditional PI control method, MPC utilizes the future output and tracking error, while the traditional PI algorithm only considers the past and present tracking errors instead of the future ones [27]-[29]. For field-weakening control, the future steady state information is important, such as stator flux and back-EMF, with which the appropriate flux or flux-producing current can be obtained. Therefore, the influence of required voltages in transient process can be suppressed effectively [30].

In this paper, the MPC method is adopted to replace the PI regulator in voltage loop to calculate the flux-producing current reference targeting the electric forklift application, in which more accurate mathematical model with the *d*-axis voltage is utilized [31]. An in-depth analysis of prediction parameter selection (prediction horizon and control horizon) is presented; additionally, the integrator is embedded in the controller inherently which can ensure zero static error. The closed-loop structure is presented where all the eigenvalues are calculated. The parameter selection principle is elaborated such the amplitude of largest eigenvalue can maintain constant in the field-weakening region. Both simulation and experimental results are provided.

The paper is organized as follows. Section II describes the IM modeling and field-weakening scheme. In Section III, the augmented state equations for current and back-EMF are established followed by the details of the MPC based field-weakening controller. Section IV presents the constrains and performance evaluation. The parameters selection is discussed based on the largest eigenvalue of voltage closed loop. Section V and VI give the simulation and experimental results validating the effectiveness of the proposed approaches. The conclusion is drawn in the section VII.

II. Field-Weakening Control for Low Voltage IM

A. IM Mathematical Model in IFOC

The dynamic models of the induction motor in rotor flux reference frame established based on the indirect field oriented control (IFOC) are

$$\begin{aligned} u_{sd} &= R_s i_{sd} + p\varphi_{sd} - \omega_s \varphi_{sq} \\ u_{sq} &= R_s i_{sq} + p\varphi_{sq} + \omega_s \varphi_{sd} \\ u_{rd} &= R_r i_{rd} + p\varphi_{rd} - (\omega_s - \omega_r)\varphi_{rq} = 0 \\ u_{rq} &= R_r i_{rq} + p\varphi_{rq} + (\omega_s - \omega_r)\varphi_{rd} = 0 \end{aligned} \tag{1}$$

The stator and rotor flux equations are

$$\begin{aligned} \varphi_{sd} &= L_s i_{sd} + L_m i_{rd} \\ \varphi_{sq} &= L_s i_{sq} + L_m i_{rq} \\ \varphi_{rd} &= L_r i_{rd} + L_m i_{sd} \\ \varphi_{rq} &= L_r i_{rq} + L_m i_{sq} = 0 \end{aligned} \tag{2}$$

where u_{sd}, u_{sq}, i_{sd}, i_{sq}, φ_{sd}, φ_{sq} are *d-q* components of the stator voltage, current and flux; u_{rd}, u_{rq}, i_{rd}, i_{rq}, φ_{rd}, φ_{rq} are *d-q* components of the rotor voltage, current and flux; ω_s is the synchronic angular speed; ω_r is the rotor angular speed; L_s is stator self-inductance; L_r is rotor self-inductance; L_m is the mutual inductance; R_s is stator resistance; R_r is rotor resistance; p is the differential operator. The torque equation is

$$T_e = 1.5 p_n \frac{L_m}{L_r} i_{sq} \varphi_{rd} \tag{3}$$

where p_n is the number of pole pairs.

B. IM Operation Region

The stator voltage limitation for IM can be written as

$$i_{sd}^2 + \sigma^2 i_{sq}^2 \le \left(\frac{V_{\max}}{\omega_s L_s} \right)^2 \tag{4}$$

where σ=1-L_m^2/($L_s L_r$) is the total leakage factor. In steady state, the rotor flux φ_{rd} is equal to $L_m i_{sd}$. The torque (3) becomes

$$T_e = 1.5 p_n \frac{L_m^2}{L_r} i_{sd} i_{sq} \tag{5}$$

The maximum torque in steady state considering the constraint (4) occurs with

$$i_{sq} = i_{sd} / \sigma \tag{6}$$

At the same time, the current limitation can be expressed as

$$i_{sd}^2 + i_{sq}^2 \le I_{\max}^2 \tag{7}$$

where I_{max} is the maximum current decided by inverter current and machine rated current. In IFOC, the motor operation is mostly related to the values of i_{sd} and i_{sq}, which are also named as flux-producing and torque-producing components of the stator current. The constraints (4) and (7) are shown in Fig.1.

When the motor speed is below the base speed ω_b, the i_{sd} reference is equal to the rated value. The segment A-B is called the constant-torque region, in which the back-EMF is less than V_{max}. When the motor speed exceeds ω_b, the operating point is decided by both (4) and (7). The maximum torque is on the segment B-C, which is the constant-power region. The line O-C represents (6) where maximum torque is obtained when the speed is beyond ω_c. If the motor operating point moves along

This article has been accepted for publication in a future issue of this journal, but has not been fully edited. Content may change prior to final publication. Citation information: DOI 10.1109/TIA.2017.2787994, IEEE Transactions on Industry Applications

segment C-D, the torque cannot be maximized and unexpected speed oscillations will occur.

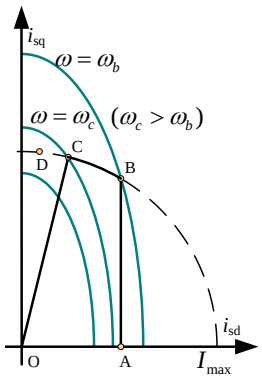

Fig.1. IM operating condition in the i_{sd} – i_{sq} plane.

C. Field-weakening Strategy

The control scheme presented in this paper, which is shown in Fig. 2, is composed of two parts: conventional IFOC module and field-weakening control. The traditional field-weakening method is based on $|\omega_{base}|/|\omega_r|$, which is sensitive to V_{dc} and parameter variation. One modified scheme of traditional algorithm is shown in Fig. 3.

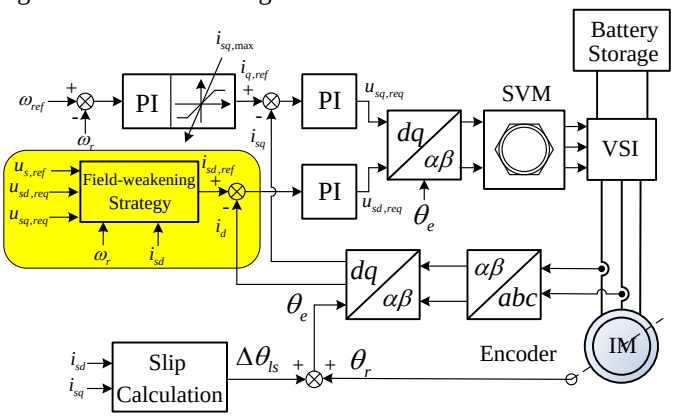

Fig.2.IM control scheme for transaction vehicle.

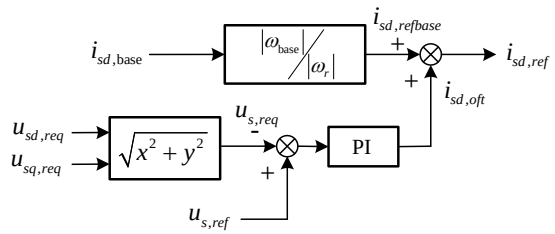

Fig.3. Control scheme with voltage closed loop.

In Fig. 3, the per unit *d*-axis current reference $i_{sd,ref}$ is obtained (by $1/\omega_r$) and then adjusted by PI regulator. When the required stator voltage $u_{s,req}$ is smaller than $u_{s,ref}$, which is set to be proportional to the DC-link voltage V_{dc}, the offset value $i_{sd,oft}$ is zero because the maximum positive output of PI regulator is set as zero. When $u_{s,req}$ becomes larger than $u_{s,ref}$, the $i_{sd,oft}$ is negative. And the $i_{d,ref}$ decreases until $u_{s,req}$ is equal to V_{dc}. In this scheme, only the voltages, which are the output of current PI regulators, are required. This algorithm is robust to motor parameters, but is easily disturbed by the unexpected variation of the DC-link voltage which is unavoidable in electric forklift applications.

III. MPC BASED FIELD-WEAKENING CONTROL

The parameter tuning of extra voltage loop in Fig.3 is difficult and usually conducted in an empirical way. Besides, as the control loop bandwidth varies with respect to the rotor speed, an inconsistent system performance will result in the entire field-weakening region.

In this paper, a MPC based controller is presented to suppress the influence of undesired disturbance from required voltage, where the augmented mathematical model is established and the optimal solution is calculated with a cost function. The guidelines for parameter tuning are discussed according to the voltage closed-loop performance.

A. Prediction Model

In the current loop control, with PI regulator and forward compensation, the closed-loop transfer function of i_d can be described as

$$i_{sd}(s) = \frac{1}{\tau_c s + 1} i_{sd,ref}(s) \tag{8}$$

where τ_c is the time constant of current loop, and it is determined by the parameters of current PI regulator. From (1) and (2), the flux φ_{sd} can be expressed as

$$\varphi_{sd}(s) = L_s \frac{\sigma\tau_r s + 1}{\tau_r s + 1} i_{sd}(s) \tag{9}$$

where τ_r=L_r/R_r is rotor time constant. The differential forms of (8) and (9) are

$$\frac{d}{dt} i_{sd} = -\frac{1}{\tau_c} i_{sd} + \frac{1}{\tau_c} i_{sd,ref} \tag{10}$$

$$\frac{d}{dt} \varphi_{sd} = -\frac{1}{\tau_r} \varphi_{sd} + \sigma L_s \frac{d}{dt} i_{sd} + \frac{L_s}{\tau_r} i_{sd} \tag{11}$$

Equations (10) and (11) are discretized with the modified Euler principle to ensure the relative degree is 1 [32]. The discrete model of equation (10) is

$$i_{sd}(k+1) = (1 - \frac{T_s}{\tau_c}) i_{sd}(k) + \frac{T_s}{\tau_c} i_{sd,ref}(k) \tag{12}$$

where T_s is the sampling period. By substituting (10) into (11), the discrete equation of φ_{sd} is

$$\varphi_{sd}(k+1) = (1 - \frac{T_s}{\tau_r}) \varphi_{sd}(k) + \frac{T_s L_s}{\tau_r} (1 - \frac{\sigma\tau_r}{\tau_c}) i_{sd}(k) + \frac{\sigma T_s L_s}{\tau_c} i_{sd,ref}(k) \tag{13}$$

The stator voltage is composed of *d*-axis and *q*-axis voltage components

$$u_s = \sqrt{u_{sd}^2 + u_{sq}^2} \tag{14}$$

The small-signal model can be expressed as

$$\Delta u_s = \frac{\partial u_s}{\partial u_{sq}} \Delta u_{sq} \tag{15}$$

Δu_{sd} is neglected in (15).The voltage u_{sq} is the main component of u_s in (14). From steady state perspective, when the motor enters the field-weakening region, the i_{sq} can be assumed to be unchanged or changing slowly, which is reasonable since i_{sq} cannot be driven to a higher level due to the voltage limitation. The flux φ_{sq} changes are the same as i_{sq} changes resulting in small Δu_{sd}.

This article has been accepted for publication in a future issue of this journal, but has not been fully edited. Content may change prior to final publication. Citation information: DOI 10.1109/TIA.2017.2787994, IEEE Transactions on Industry Applications

The equation (15) is rewritten as

$$\Delta u_s(k) = \frac{\partial u_s}{\partial u_{sq}} \Delta u_{sq}(k) = m_k \Delta u_{sq}(k) \tag{16}$$

where the coefficient m_k is defined as

$$m_k = \frac{\partial u_s}{\partial u_{sq}} = \frac{u_{sq}}{\sqrt{u_{sd}^2 + u_{sq}^2}} \tag{17}$$

With the incremental form of (13), the equation (16) is expressed as

$$\begin{aligned} \Delta u_s(k+1) = (1-\frac{T_s}{\tau_r})\Delta u_s(k) + m_k \omega_s \Bigg[\frac{T_s L_s}{\tau_r}(1-\frac{\sigma\tau_r}{\tau_c})\Delta i_{sd}(k) \\ + \frac{\sigma T_s L_s}{\tau_c} \Delta i_{sd,ref}(k) \Bigg] \end{aligned} \tag{18}$$

B. Augmented State Equation

Equations (12) and (18) constitute the incremental state equation as

$$\begin{aligned} \Delta \boldsymbol{x}_m(k+1) &= \boldsymbol{A}_m \Delta \boldsymbol{x}_m(k) + \boldsymbol{B}_m \Delta u_{MPC}(k) \\ y(k) &= \boldsymbol{C}_m \boldsymbol{x}_m(k) \end{aligned} \tag{19}$$

where $\boldsymbol{x}_m(k)=[i_{sd}(k)\ u_s(k)]^{\mathrm{T}}$, $\Delta\boldsymbol{x}_m(k)=\boldsymbol{x}_m(k)-\boldsymbol{x}_m(k\text{-}1)$, $y(k)=u_s(k)$, $u_{MPC}(k)=i_{sd,ref}(k)$, $\Delta u_{MPC}(k)=u_{MPC}(k)-u_{MPC}(k\text{-}1)=\Delta i_{sd,ref}(k)$. The matrix $\boldsymbol{A}_m$, $\boldsymbol{B}_m$ and $\boldsymbol{C}_m$ are

$$\boldsymbol{A}_m = \begin{bmatrix} 1-\frac{T_s}{\tau_c} & 0 \\ \frac{m_k \omega_s T_s L_s}{\tau_r}\left(1-\frac{\sigma\tau_r}{\tau_c}\right) & 1-\frac{T_s}{\tau_r} \end{bmatrix}, \ \boldsymbol{B}_m = \begin{bmatrix} \frac{T_s}{\tau_c} \\ \frac{m_k \omega_s \sigma T_s L_s}{\tau_c} \end{bmatrix},$$

$$\boldsymbol{C}_m = \begin{bmatrix} 0 & 1 \end{bmatrix}.$$

The equation (19) cannot be utilized for model prediction directly because $\Delta\boldsymbol{x}_m(k)$ is not included in the output equation. The augmented form of (19) is established by combining the states $\boldsymbol{x}_m(k)$ and $y(k)$ as

$$\begin{aligned} \boldsymbol{x}(k+1) &= \boldsymbol{A}\boldsymbol{x}(k) + \boldsymbol{B}\Delta u_{MPC}(k) \\ y(k) &= \boldsymbol{C}\boldsymbol{x}(k) \end{aligned} \tag{20}$$

where $\boldsymbol{x}(k)$ is the new state variable augmented from $\boldsymbol{x}_m$ and $y(k)$, as $\boldsymbol{x}(k)==[\Delta\boldsymbol{x}^{\mathrm{T}}{}_m(k)\ \ y(k)]^{\mathrm{T}}$. The matrix $\boldsymbol{A}$, $\boldsymbol{B}$ and $\boldsymbol{C}$ are

$$\boldsymbol{A} = \begin{bmatrix} \boldsymbol{A}_m & 0 \\ \boldsymbol{C}_m\boldsymbol{A}_m & 1 \end{bmatrix}, \ \boldsymbol{B} = \begin{bmatrix} \boldsymbol{B}_m \\ \boldsymbol{C}_m\boldsymbol{B}_m \end{bmatrix}, \ C = [0 \quad 0 \quad 1].$$

C. MPC Solution

The input and output vectors of the MPC solution is defined as following:

$$\Delta\boldsymbol{U}_{MPC} = [\Delta u_{MPC}(k) \quad \Delta u_{MPC}(k+1) \quad \cdots \quad \Delta u_{MPC}(k+N_c-1)]^{\mathrm{T}} \tag{21}$$

$$\boldsymbol{Y} = [y(k+1) \quad y(k+2) \quad \cdots \quad y(k+N_p)]^{\mathrm{T}} \tag{22}$$

where N_c is called the control horizon and N_p is called the prediction horizon. $N_c \leqslant N_p$ and $\Delta u_{MPC}(k+j)$ is zero when $N_c\text{-}1<j<N_p$. From (20), the relationship between $\boldsymbol{Y}$, $\Delta\boldsymbol{U}_{MPC}$ and $\boldsymbol{x}(k)$ is formulated as

$$\boldsymbol{Y} = \boldsymbol{F}\boldsymbol{x}(k) + \boldsymbol{\Phi}\Delta\boldsymbol{U}_{MPC} \tag{23}$$

where

$$\boldsymbol{F} = \begin{bmatrix} \boldsymbol{CA} \\ \boldsymbol{CA}^2 \\ \vdots \\ \boldsymbol{CA}^{Np} \end{bmatrix}, \ \boldsymbol{\Phi} = \begin{bmatrix} \boldsymbol{CB} & 0 & \cdots & 0 \\ \boldsymbol{CAB} & \boldsymbol{CB} & \cdots & 0 \\ \vdots & \vdots & & \vdots \\ \boldsymbol{CA}^{N_p-1}\boldsymbol{B} & \boldsymbol{CA}^{N_p-2}\boldsymbol{B} & \cdots & \boldsymbol{CA}^{N_p-N_c}\boldsymbol{B} \end{bmatrix}.$$

The cost function is defined as

$$\begin{aligned} J &= \sum_{j=1}^{N_p} \left\| r(k) - \mathrm{y}(k+i) \right\|_2^2 + k_u \sum_{j=1}^{N_c} \left\| \Delta u_{MPC}(k+j-1) \right\|_2^2 \\ &= \left(\boldsymbol{R}_p - \boldsymbol{Y} \right)^{\mathrm{T}} \left(\boldsymbol{R}_p - \boldsymbol{Y} \right) + \Delta\boldsymbol{U}_{MPC}^{T} \boldsymbol{K}_u \Delta\boldsymbol{U}_{MPC} \end{aligned} \tag{24}$$

where $r(k)$ is the voltage reference at time k and is supposed to be constant from time k to $k+N_p$. $\boldsymbol{R}_p = r(k)\ [1\ 1\ \ldots\ 1]^{\mathrm{T}}$ is the reference vector. k_u is the weight coefficient to be tuned by closed-loop performance and $\boldsymbol{K}_u = k_u \boldsymbol{I}_{Nc\times Nc}$ is weight matrix. The optimal solution is obtained by minimizing J and is calculated from $\partial J/\partial \boldsymbol{U}_{MPC}=0$ as

$$\Delta\boldsymbol{U}_{MPC} = \left(\boldsymbol{\Phi}^{\mathrm{T}}\boldsymbol{\Phi} + \boldsymbol{K}_u \right)^{-1} \boldsymbol{\Phi}^{\mathrm{T}} \left(\boldsymbol{R}_p - \boldsymbol{F}\boldsymbol{x}(k) \right) \tag{25}$$

In (25), total N_c optimal control signals are calculated. With the receding horizon control (RHC) principle, only the first sample of this sequence $\Delta u_{MPC}(k)$ is utilized for k period. The control signal with non-incremental form is calculated as

$$i_{sd,ref}(k) = i_{sd,ref}(k-1) + \Delta u_{MPC}(k) \tag{26}$$

In the next sample period, the new measurement is taken to form the state vector for the calculation of the new sequence of control signal. And the formula (25) plus (26) are repeated for $i_{sd,ref}(k+1)$.

IV. MPC Algorithm Implementation

The augmented state equation is established for IM field-weakening control where the input and output of controller are incremental. The MPC constraint and parameter selection consideration is discussed as this is critical for algorithm implementation.

The analysis of stability degree about MPC is much more complex than conventional PI controller. In this paper, a simplified but effective method is presented. All the closed-loop eigenvalues are evaluated and the largest one is utilized to evaluate the performance. The controller parameters are selected in view of the closed-loop performance.

A. MPC based Field-weakening Scheme

MPC algorithms allow the integration of system constraints in the controller design. In (20), only the constrains of control variable need to be considered, including incremental variation and amplitude as

$$\left| \Delta u_{MPC}(k) \right| \leq I_{sd,\Delta\max} \tag{27}$$

$$I_{sd,\min} \leq u_{MPC}(k) \leq I_{sd,\mathrm{rated}} \tag{28}$$

where $I_{sd,rated}$ is the rated flux-producing current, $I_{sd,min}$ is the minimum value of i_{sd}, and $I_{sd,\Delta max}$ is the maximum incremental variation.

The new field-weakening algorithm based on MPC is presented to replace the modified scheme of traditional algorithm, as shown in Fig.4.The u_s^* is the reference of voltage loop, which is set as high as possible to maximize the

This article has been accepted for publication in a future issue of this journal, but has not been fully edited. Content may change prior to final publication. Citation information: DOI 10.1109/TIA.2017.2787994, IEEE Transactions on Industry Applications

electromagnetic torque. The increment of voltage u_s and d-axis current i_{sd} are calculated as the input to the controller, while the output is the first sample of optimal sequence. The increment of d-axis current reference should be limited by the constrains (27). And the result of the integration module $1/(1\text{-}z^{-1})$ is the amplitude of d-axis current reference which is limited by the constrains (28). Similar to the PI regulator, the anti-windup function is essential in the integration module.

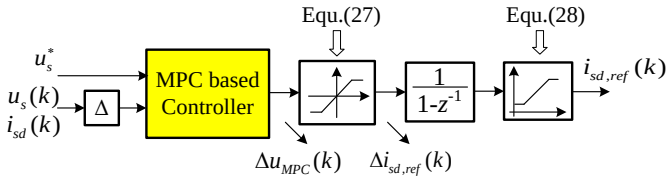

Fig.4. MPC based IM field-weakening strategy.

B. Closed-loop Evaluation

The closed-loop stability analysis of MPC is complex, especially when the prediction horizon N_p is chosen to be large [30]. Fortunately, if N_p and N_c are determined, the closed-loop control has the explicit feedback structure, which can simplify the analysis.

According to MPC algorithm and RHC principle, the first element of ΔU_{MPC} can be described as:

$$\Delta u_{MPC}(k) = K_y r(k) - \boldsymbol{K}_{mpc} x(k) \tag{29}$$

where K_y is the first element of $(\boldsymbol{\Phi}^T\boldsymbol{\Phi}+\boldsymbol{K}_u)^{-1}\boldsymbol{\Phi}^T\boldsymbol{R}_p$. $\boldsymbol{K}_{mpc}$ is the first row of $(\boldsymbol{\Phi}^T\boldsymbol{\Phi}+\boldsymbol{K}_u)^{-1}\boldsymbol{\Phi}^T\boldsymbol{F}$, and $\boldsymbol{K}_{mpc}=[K_x \;\; K_y]$. The closed-loop structure is shown in Fig. 5.

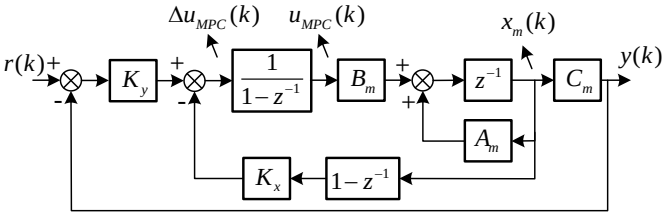

Fig.5. MPC closed-loop structure.

By substituting (29) into (20), the closed-loop equation is

$$\begin{aligned} x(k+1) &= \boldsymbol{A}x(k) + \boldsymbol{B}(K_y r(k) - \boldsymbol{K}_{mpc} x(k)) \\ &= (\boldsymbol{A} - \boldsymbol{B}\boldsymbol{K}_{mpc})x(k) + \boldsymbol{B}K_y r(k) \end{aligned} \tag{30}$$

The closed-loop eigenvalues can be evaluated through the characteristic equation of (30), as

$$\det\left[\lambda \boldsymbol{I} - (\boldsymbol{A} - \boldsymbol{B}\boldsymbol{K}_{mpc})\right] = 0 \tag{31}$$

The dimension of $\boldsymbol{A}$ is three, and thus, there are three eigenvalues of (31). Analytical solutions of (31) are difficult to derive because of the combination variety of N_p and N_c. If the N_p and N_c are defined, the matrix $\boldsymbol{K}_{mpc}$ and all the eigenvalues can be calculated with Matlab toolbox.

C. Parameter Selection

Theoretically, the loop is stable if all the eigenvalues are inside the unit circle. The eigenvalue with largest amplitude has the greatest impact on the system. There are three eigenvalues of (30) defined as λ_1, λ_2 and λ_3. The largest eigenvalue is defined as

$$\lambda_{\max} = \max\left\{|\lambda_1|, |\lambda_2|, |\lambda_3|\right\} \tag{32}$$

In optimal solution equation (24), the weight coefficient k_u is an important parameter, by which the close-loop performance is influenced directly. If the k_u and coefficient matrices are constant, the eigenvalues will be constant too. But in the state equation (20), the coefficient m_k and angular speed ω_s in matrix A are time-variant. The eigenvalues will change when the rotor speed varies.

In this scheme, the eigenvalue $\lambda_{\max}$ is utilized to evaluate the close-loop performance. The motor parameters are shown in Table I of section V. The arithmetic solution of $\lambda_{\max}$ can be calculated with Matlab.

The selection of prediction horizon N_p and the control horizon N_c is one of the important issues. The condition number of the Hessian matrix $(\boldsymbol{\Phi}^T\boldsymbol{\Phi}+\boldsymbol{K}_u)$ may increases significantly with large N_p, resulting in the numerical sensitivity which deteriorates the stability. The relation between $\lambda_{\max}$ and $m_k\omega_s$ with different N_p and N_c is shown in Fig.7. (N_p, N_c) indicates the different combination. When the N_p is constant, the $\lambda_{\max}$ with smaller N_c becomes smaller. When the N_c is constant, the $\lambda_{\max}$ with larger N_p is smaller.

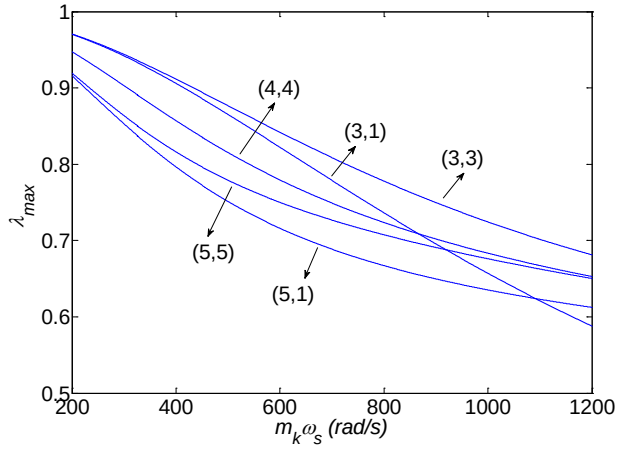

Fig.6. λ_{max} calculation with different combination of N_p and N_c when k_u=0

On the other hand, the computation complexity is decided by the dimension of $(\Phi^T\Phi+K_u)\Phi^T$, which is N_c in (25). For motor control, the amount of algorithm calculation decreases a lot when the N_c is set smaller because of the high sampling frequency. In this paper, N_p is set as 3 and N_c is set as 1 considering the calculation burden and complexity.

When k_u is constant, the relationship between $\lambda_{\max}$ and $m_k\omega_s$ is shown in Fig.7. When $m_k\omega_s$ increases, the $\lambda_{\max}$ becomes smaller and the close-loop bandwidth becomes higher, which illustrates that the response may change when the motor operates in different speed. If $m_k\omega_s$ is constant, the $\lambda_{\max}$ is inversely proportional to k_u. The close-loop bandwidth is lower when k_u is set larger, which is concordant with theoretical analyses about k_u.

The eigenvalues vary as the rotor speed changes, which is undesirable for control objective. Fortunately, the eigenvalues can be tuned with k_u to ensure constant $\lambda_{\max}$ with different speed. From Fig.6, the $\lambda_{\max}$ increases with k_u monotonically. With the numerical calculation of Matlab, k_u can be decided uniquely with the given $\lambda_{\max}$ for different $m_k\omega_s$ as shown in Fig.8 where

This article has been accepted for publication in a future issue of this journal, but has not been fully edited. Content may change prior to final publication. Citation information: DOI 10.1109/TIA.2017.2787994, IEEE Transactions on Industry Applications

curves of k_u are calculated according to different $\lambda_{\max}$ (0.8/0.9/0.92/0.95). k_u increases with $m_k\omega_s$ monotonically with the given $\lambda_{\max}$, which can be tuned based on the performance obtained from simulation and experiments.

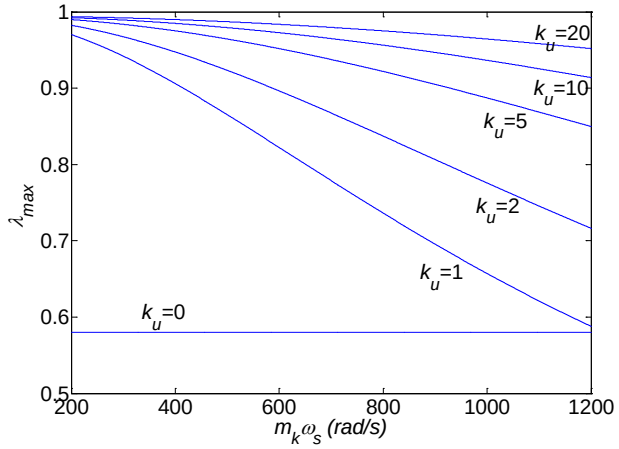

Fig.7. λ_{max} calculation with constant k_u when N_p=3 and N_c=1

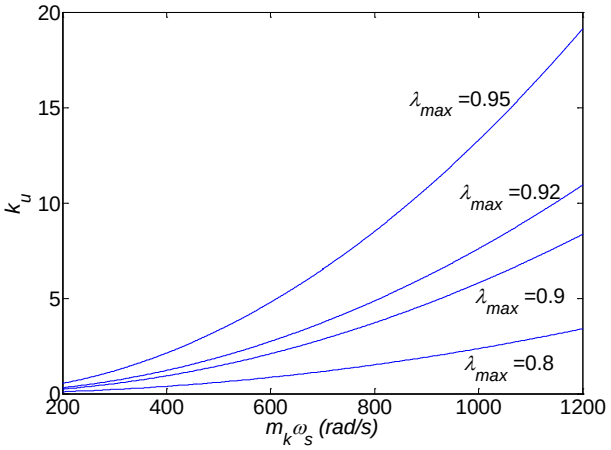

Fig.8. k_u calculation with constant λ_{max} when N_p=3 and N_c=1

V. Simulation Analysis

The proposed MPC based field-weakening strategy is simulated with Matlab/simulink to validate the effectiveness. The machine and control parameters are listed in Table I.

TABLE I

Induction Machine and Control Parameters

Rated power (kW)	9
Rated voltage (V)	58
Rated current (A)	149
Rated speed (RPM)	1200
Rated frequency (Hz)	62
Max speed (RPM)	3000
R_s**(mΩ)**	20.3
R_r**(mΩ)**	26.3
L_s **(mH)**	2.629
L_r **(mH)**	2.622
L_m **(mH)**	2.498
p_n	3
Connection	△
I_{sdn}**(A)(peak)**	133
$I_{sd,\Delta max}$**(A)**	0.2
N_p	3
N_c	1

The results of ramp response without load are shown in Fig.9. The speed reference and stator voltage u_s response are shown in Fig.9(a). The speed begins to increase at 1s, 3s, 5s and 7s with the same increment of speed reference of 500rpm. The acceleration is 500rpm/s, which is set bigger than the requirement of electric forklift. The reference $u_{s,ref}$ is calculated from

$$u_{s,ref} = k_{dc}\frac{\sqrt{3}}{2}\frac{2}{3}V_{dc} = \frac{k_{dc}}{\sqrt{3}}V_{dc} \tag{33}$$

And the reference should be less than the maximum value. The coefficient k_{dc} is set as 0.95 in this paper. In Fig.9, V_{dc} is 60V and $u_{s,ref}$ is 33V. In voltage loop, the feedback is the required stator voltage $u_{s,req}$. In Fig.9(a), $u_{s,req}$ reaches the set value when the speed exceeds 800rpm and the field-weakening strategy becomes effective. In the acceleration process, $u_{s,ref}$ is tracked well. At the start and end of the acceleration, the change rate of q-axis current becomes larger because of the speed regulator. More q-axis voltage is required in short time, which results in the peaks of $u_{s,req}$.

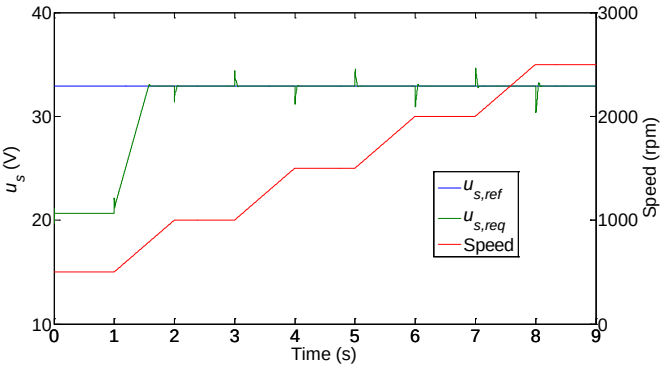

(a)

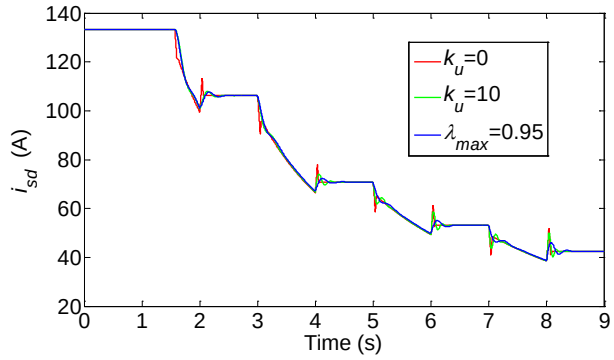

(b)

Fig.9. Ramp response without load (a) speed and u_s (b) i_{sd}

The i_{sd} responses with different MPC parameters are shown in Fig.9(b). In the process of acceleration, the $i_{sd,ref}$ decreases steadily. The peaks of $u_{s,req}$ disturb the $i_{sd,ref}$ calculation severely. The undesired disturbance of $i_{sd,ref}$ is large and harmful. When k_u is zero, the amplitude of the disturbance in each start and end are almost the same. The λ_{max} with k_u=10 is larger than k_u=0 and $\lambda_{\max}$ is not constant when the speed varies.

In low speed region, λ_{max} is larger and the response of voltage controller is slower. The influence of $u_{s,req}$ peaks can be suppressed effectively. At higher speeds, λ_{max} changes to a

This article has been accepted for publication in a future issue of this journal, but has not been fully edited. Content may change prior to final publication. Citation information: DOI 10.1109/TIA.2017.2787994, IEEE Transactions on Industry Applications

smaller value and the response becomes faster, which results in larger disturbance amplitude.

In order to ensure the constant response with different speed, the scheme with constant λ_{max} is adopted. In Fig.9(a), λ_{max} is set as 0.95. In each sampling period, the rotor speed ω_r is measured, and ω_s plus m_k are calculated. The response is almost the same at 2s, 4s, 6s and 8s. Compared with k_u=0, the influence of $u_{s,req}$ peaks can be suppressed effectively, which is important in the application of traction EV or electric forklift.

VI. Experimental Results

The proposed field-weakening control was experimentally tested on a inverter-fed IM drive bench. The machine and control parameters are the same as those listed in Table I. The experimental setup is shown in Fig.10. The induction motor is coupled with a30-kW load motor. The total inertia is much larger than the one in simulation. The controller is supplied by a DC power without energy feedback. The V_{dc} is increased when the motor decelerates with large inertia. The MPC algorithm is implemented in the 32-bit processor XMC4500. The PWM frequency is 10kHz. The sampling frequency of field-weakening control is 1kHz.

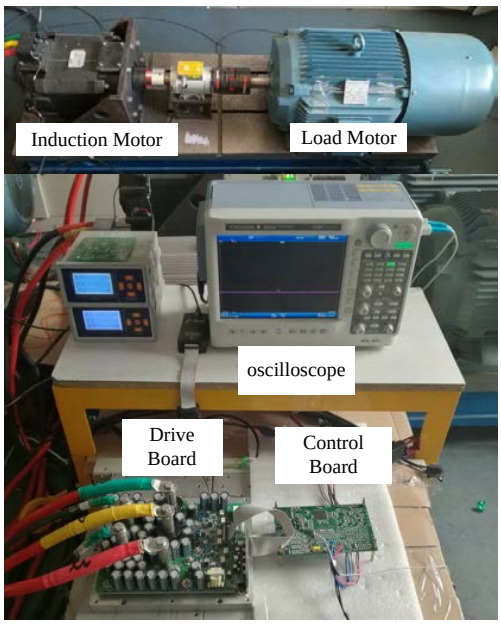

Fig.10. Experimental setup of inverter-fed IM drive

The response with conventional PI regulator is shown in Fig.11. The motor speed starts to increase from 500rpm to 1500rpm in 1s intervals up to 2500rpm in 9s. The acceleration is 250rpm/s. The nominal V_{dc} is 60V. In Fig.11(a), the speed is tracked well with negligible overshoot because the speed is controlled with a PI regulator.

In Fig.11(b), the $i_{sd,ref}$ starts to decrease at 2s and decreases further as speed increases. In the speed overshoot process, V_{dc} is increased beyond the DC power capacity and is released with resistor. The V_{dc} fluctuation results in the undesired oscillations in $i_{sd,ref,}$. In other words, the $i_{sd,ref}$ is much sensitive to the DC-link variation.

Fig.11(c) shows the reference and feedback of u_s. The reference is set as 33V which is equal to the simulation. The u_s is controlled well in the field-weakening region except the V_{dc} fluctuation area. The phase current i_A is shown in Fig.11(d), the amplitude of which is consistent with the $i_{sd,ref}$.

The typical field-weakening analysis is discussed in [10], where the q-axis voltage u_{sq} are considered, and the d-axis voltage u_{sd} is neglected. This approximation is not reasonable when a deep field weakening happens and the deteriorate performance will be resulted. In Fig.11, the PI parameters are tuned based on a trial and error method.

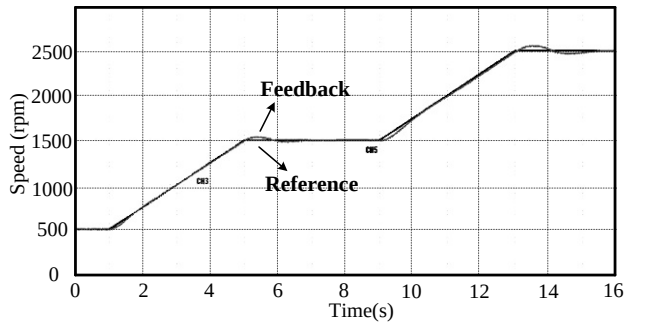

(a)

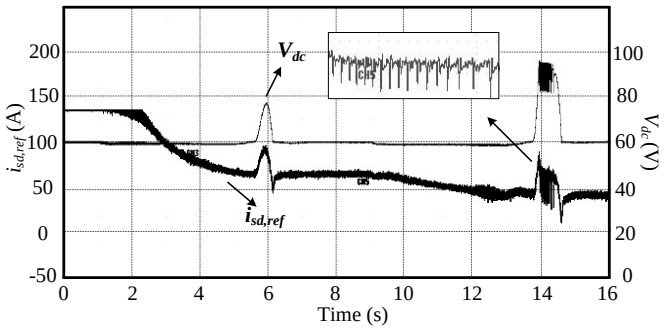

(b)

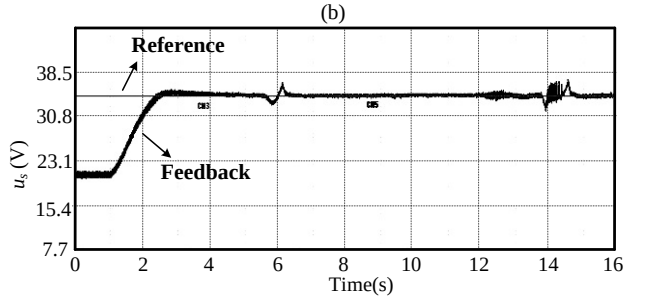

(c)

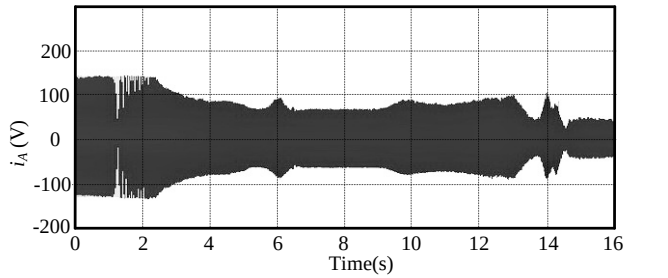

(d)

Fig.11.Field-weakening response with conventional PI regulator (k_p = 9.35 and k_i = 45.83) (a) speed reference and feedback (b) $i_{sd,ref}$ and V_{dc} (c) u_s reference and response (d) phase current i_A

This article has been accepted for publication in a future issue of this journal, but has not been fully edited. Content may change prior to final publication. Citation information: DOI 10.1109/TIA.2017.2787994, IEEE Transactions on Industry Applications

The response of MPC algorithm with λ_{max} = 0.95 is shown in Fig.12. The speed reference is set as the same as in Fig.11. The $i_{sd,ref}$ is also influenced by the V_{dc} fluctuation. In Fig.12(b), there is no oscillation in $i_{sd,ref}$ at 14s, which is much better than Fig.11(b). In Fig.12(c), the u_s is also tracked well in most field-weakening region except the V_{dc} rising area where the u_s control error is larger than Fig.11(c). The result is consistent with previous analysis. In Fig.12, λ_{max} is set as 0.95 and the system responses relatively slowly. The controlled u_s is not as sensitive to V_{dc} variation as that with PI regulator. Although the u_s shows some tracking error, there is no oscillation in $i_{sd,ref}$, which is very important in field-weakening control.

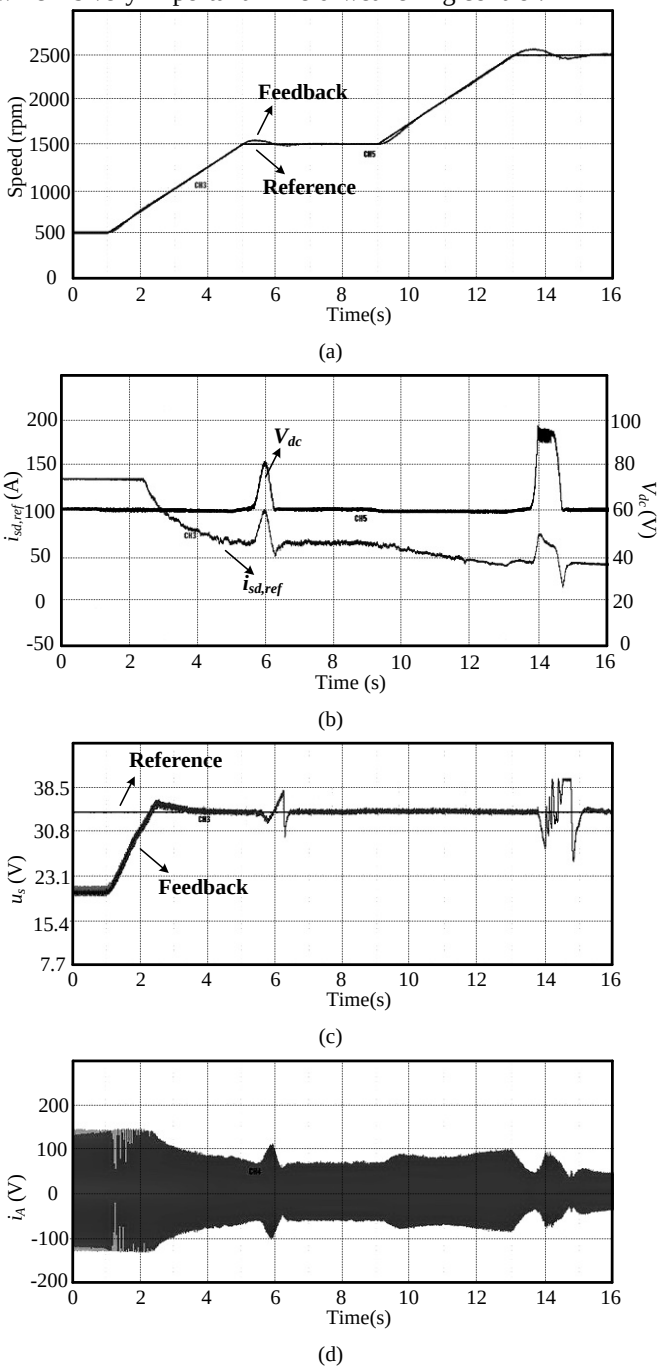

Fig.12.Field-weakening response based on MPC controller with λ_{max} = 0.95 (a) speed reference and feedback (b) $i_{sd,ref}$ and V_{dc} (c) u_s reference and response (d) phase current i_A

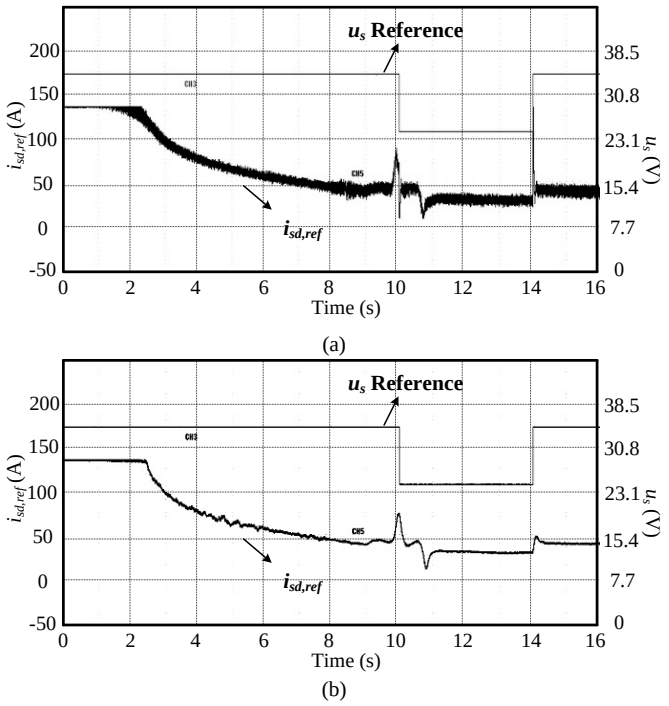

Fig.13.u_s step response with different algorithms (a) PI regulator (k_p = 9.35 and k_i = 45.83) (b) MPC with λ_{max} = 0.95

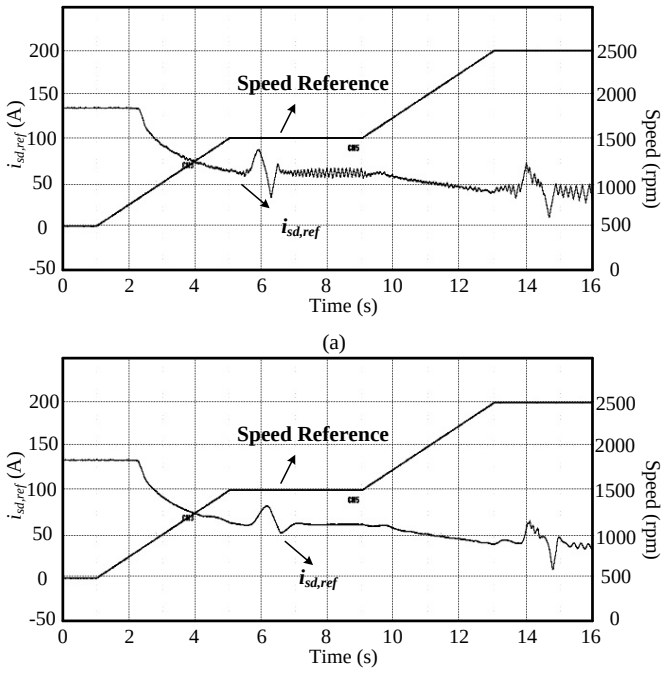

Fig.14.i_{sd} response based on MPC controller (a) k_u=0 (b) k_u=10

This analysis is also illustrated in Fig.13 where the step responses are shown with different algorithms. The motor starts to accelerate from 500rpm at 1s and reaches 2500rpm at 9s. And the u_s reference decreases at 10s and changes back at14s.In the acceleration process, the two algorithms have almost the same response to decrease the field flux. The curve is a little wider in Fig.13(a) because of the proportional function in the PI regulator. When the u_s changes in deep field-weakening region, the responses of two methods differ obviously. In Fig.13(a),

This article has been accepted for publication in a future issue of this journal, but has not been fully edited. Content may change prior to final publication. Citation information: DOI 10.1109/TIA.2017.2787994, IEEE Transactions on Industry Applications

there are two peaks at 10s and 14s, which are undesired in electric vehicles. And the peaks are eliminated in Fig.13(b) and $i_{sd,ref}$ responses to the proper value quickly. And the responses are not the same comparing the step-down and step-up process due to the u_q influence.

In comparison, the responses of MPC algorithm with fixed k_u are shown in Fig.14with λ_{max} = 0.95. When k_u = 0 the λ_{max} is smallest in all the speed regions and the response is the fastest. In Fig.14(a), the $i_{sd,ref}$ has oscillations in steady state in 1500rpm and 2500rpm. When k_u = 10, the λ_{max} is big in low speed region and becomes smaller with higher speed. There is no oscillation in 1500rpm but appears in 2500rpm, which is shown in Fig.14(b).

It is seen from the comparison of three MPC methods (k_u = 0, k_u = 10, and λ_{max} = 0.95) that the λ_{max} plays an important role in u_s control and constant λ_{max} can ensure a consistent response in all the field-weakening regions, which is important in electric vehicle applications.

For electric forklift, the maximum motor speed is typically 2 to 3 times of the base speed. The PI parameters, calculated following [10], cannot be adapted without modification since the u_{sd} is neglected and the ratio of u_{sd} changes with respect to various speed. The motor cannot follow the speed reference during the acceleration if the bandwidth is insufficient. If the bandwidth is set bigger, the oscillation occurs frequently in the high speed region. Thus the parameters of PI regulator are tuned in an empirical way in most cases. In the proposed MPC method, the parameter λ_{max} might change for different applications. The λ_{max} range is set between 0.92~0.98 for the u_s control of electric forklift. If the load inertia is small and a fast response is required in the field-weakening region, the λ_{max} should be set smaller.

VII. Conclusion

A model predictive control (MPC) based algorithm is developed addressing the importance of the field-weakening performance for traction IM. In steady state, the control error can be eliminated with the embedded integrator for the mathematical model. In the dynamic process, the performance is related to the eigenvalue with the largest amplitude which is calculated from the explicit closed-loop structure. According to the cost function, the relationship between the eigenvalue and the weight coefficient is built. The coefficients thus can be adjusted with the predefined eigenvalue in different speed regions, and the expected performance can be guaranteed. The simulation and experimental results and analysis validate the proposed method for both static and dynamic processes.

Compared to PI regulator, the benefits of adopting the proposed MPC method are summarized as following:

(1) In MPC, the small signal model of voltage is utilized to predict the future stator voltage us, in which the u_{sd} is considered. Compared to mathematic model used in PI regulator [10], the proposed prediction model is more precise which is modified in the real time with updated $u_{sd}(k)$ and $\omega_r(k)$. The MPC shows better performance with a more accurate model.

(2) The MPC controller is established with incremental form. The total output is smooth and is not influenced by the variation of controller parameters. However, the problem exists in PI regulators when the k_p needs to be tuned in a wide range in a short time. The MPC parameter k_u is modified in each sampling period, while the total output doesn't show step variation.

(3) Only one parameter needs to be considered: λ_{max}. Once the λ_{max} is determined, the controller shows consistent performance in the entire field-weakening region. However, there are two parameters in PI regulator and the parameter tuning is difficult for u_s control, especially when the consistent response is required for both light and deep field-weakening region.

References

[1] M. C. Di Piazza, A. Ragusa, and G. Vital, "Effects of common-mode active filtering in induction motor drives for electric vehicles," *IEEE Trans. Veh. Technol.*, vol. 59, no. 6, pp. 2664–2673, Jul. 2010.

[2] X. Zhang, "Sensorless Induction motor drive using indirect vector controller and sliding-Mode observer for electric vehicles," *IEEE Trans. Veh. Technol.*, vol. 62, no. 7, pp. 3010–3018, Sep. 2013.

[3] L. Diao, D. Sun, K. Dong, etc, "Optimized design of discrete traction induction motor model at low-switching frequency," *IEEE Trans. Power Electron.*, vol. 28, no. 10,pp. 4803–4810, May. 2013.

[4] J. L. Kirtley, R. F. Schiferl, and D. T. Peters, "The Case for induction motors with die-cast copper rotors for high efficiency traction motors," *Technical Paper of Society of Automotive Engineers*, No. 2009-01-0956, Apr. 2009.

[5] M. Zeraoulia, M. E. H.Benbouzid, and D. Diallo, "Electric motor drive selection issues for HEV propulsion systems: comparative study," *IEEE Trans. Veh. Technol.*, vol. 55, no. 6, pp. 1756–1764, Nov. 2006.

[6] M. Farasat, A. M. Trzynadlowski, and M. S. Fadali, "Efficiency improved sensorless control scheme for electric vehicle induction motors," *IET Electr. Syst. Transp.*, vol. 4, no.4, pp. 122–131, Jul. 2014.

[7] Y. Liu, J. Zhao, R. Wang, and C. Huang, "Performance improvement of induction motor current controllers in field-weakening region for Electric vehicles," *IEEE Trans. Power Electron.*, vol. 28, no. 5,pp. 2468–2482, May. 2013.

[8] G. Pellegrino, A. Vagati, B. Boazzo, etc, "Comparison of induction and PM synchronous motor drives for EV application including design examples," *IEEE Trans. Ind. Appl.*, vol. 48, no. 6, pp. 2322–2332, Nov. 2012.

[9] A. V. Ravi Teja, C. Chakraborty, S. Maiti, etc, "A new model reference adaptive controller for four quadrant vector controlled induction motor drives," *IEEE Trans. Ind. Electron.*, vol. 59, no. 10, pp. 3757–3767, Oct. 2012.

[10] D. Casadei, M. Mengoni, G. Serra, etc, "A control scheme with energy saving and DC-Link overvoltage rejection for induction motor drives of electric vehicles," *IEEE Trans. Ind. Appl.*, vol. 46,no. 4, pp. 1436–1446, Jul./Aug. 2010.

[11] D. Stojic, M. Milinkovic, S. Veinovic, etc, "Improved stator flux estimator for speed sensorless induction motor drives," *IEEE Trans. Power Electron.*, vol. 30, no. 4,pp. 2363–2371, Apr. 2015.

[12] D. Casadei, F. Profumo, G. Serra, etc, "Performance analysis of a speed-sensorless induction motor drive based on a constant switching frequency DTC scheme," *IEEE Trans. Ind. Appl.*, vol. 39, no. 2,pp. 476–484, Mar./Apr. 2003.

[13] M. H. Shin, D. S. Hyun, and S. B. Cho, "Maximum torque control of stator-flux-oriented induction machine drive in the field-weakening region," *IEEE Trans. Ind. Appl.*, vol. 38, no. 1, pp. 117–121, Jan./Feb. 2002.

[14] D. Casadei, G. Serra, A. Tani, and L. Zarri, "A robust method for field weakening operation of induction motor drives with maximum torque capability," in *Proc. IEEE IAS Annul Conf.*, Oct. 2006,pp. 111–117.

[15] L. G. Gallegos, F. S. Gunawan, and J. E. Walters, "Current control of induction machines in the field-weakened region," *IEEE Trans. Ind. Appl.*, vol. 43, no. 4, pp. 981–989, Jul./Aug. 2007.

[16] M. Mengoni, L. Zarri, A. Tani, G. Serra, and D. Casadei, "Stator flux vector control of induction motor drive in the field weakening region," *IEEE Trans. Power Electron.*, vol. 23, no. 2, pp. 981–948, Mar. 2008.
[17] M. Mengoni, L. Zarri, A. Tani, G. Serra, and D. Casadei, "A comparison of four robust control schemes for field-weakening operation of induction motors," *IEEE Trans. Power Electron.*, vol. 27, no. 1, pp. 307–32, Jan. 2012.
[18] L. Harnefors, K. Pietilainen, and L. Gertmar, "Torque-maximizing field-weakening control: design, analysis, and parameter selection," *IEEE Trans. Ind. Electron.*, vol. 48, no. 1, pp. 161–168, Feb. 2001.
[19] D. M. Ionel, M. Popescu, S. J. Dellinger, etc, "On the variation with flux and frequency of the core loss coefficients in electrical machines," *IEEE Trans. Ind. Appl.*, vol. 42, no. 3,pp. 658–667, May/Jun. 2006.
[20] H. Liu, Z. Q. Zhu, E. Mohamed, Y. Fu, and X. Qi, "Flux-weakening control of non-salient pole PMSM having large winding inductance, accounting for resistive voltage drop and inverter nonlinearities," *IEEE Trans. Power .Electron.*, vol. 27, no. 2, pp. 942–952, Feb. 2012.
[21] Z. Yin, C. Zhao, Y. Zhong, and J. Liu, "Research on robust performance of speed-sensorless vector control for the induction motor using an interfacing multiple-model extended kalman filter," *IEEE Trans. Power. Electron.*, vol. 29, no. 6, pp.3011–3019, Jun. 2014.
[22] S. Carpiuc, and C. Lazzr, "Fast real-time constrained predictive current control in permanent magnet synchronous machine-based automotive traction drives," *IEEE Trans. Transportation Electrification*, vol. 1, no. 4, pp. 326–335, DEC. 2015.
[23] T. Geyer, "Model predictive direct torque control: derivation and analysis of the state-feedback control law," *IEEE Trans. Ind. Appl.*, vol. 49, no.5, pp. 2146–2157, Sep./Oct. 2013.
[24] K. Belda, and D. Vosmik, "Explicit generalized predictive algorithms for speed control of PMSM drives," *IEEE Trans. Ind. Electron.*, vol. 63, no.6, pp. 3889–3896, Jun. 2016.
[25] L. Wang, S. Chai, E. Rogers, etc, "Multivariable repetitive-predictive controllers using frequency decomposition," *IEEE Trans. System Technology*, vol. 20, no. 6,pp. 1597–1604, Nov. 2012.you
[26] A. Darba, F. D. Belie, P. Dhaeseand J. A. Melkebeek, "Improved dynamic behavior in BLDC drives using model predictive speed and current control," *IEEE Trans. Ind. Electron.*, vol. 63, no. 2, pp. 728–740, Feb. 2016.
[27] M. Preindl, "Robust control invariant sets and Lyapunov-based MPC for IPM synchronous motor drives," *IEEE Trans. Ind. Electron.*, vol. 63, no. 6,pp. 3925–3933, Jun. 2016.
[28] H. A. Young, M. A. Perez, J. Rodriguez, and H. Abu-Rub. "Assessing finite-control-set model predictive control: A comparison with a linear current controller in two-level voltage source," *IEEE Industrial Electronics Magazine*, vol. 8, no. 1, pp. 44-52, Mar.2014.
[29] M. Preindl, "Novel model predictive control of a PM synchronous motor drive," *Ph.D. dissertation*, University of Padua, 2014
[30] S. Chai, L. Wang, and E. Rogers, "A cascade MPC control structure for a PMSM with speed ripple minimization," *IEEE Trans. Ind. Electron.*, vol. 60, no. 8,pp. 2978–2987, Aug. 2013.
[31] J. Su, R. Gao, and I. Husain, "Model predictive control based field-weakening strategy for traction EV used induction motor," in *Proc IEEE ECCE*, Milwaukee, U.S.A., 2016.
[32] C. A. Silva, and J. I. Yuz, "On sampled-data models for model predictive control," in *Proc IEEE Ind. Electron. Conf. (IECON)*,Glendale, U.S.A., 2010, pp. 2966–2971.

Jianyong Su (M'15) was born in China, in 1979. He received his B.S., M.S., and Ph.D. in Electrical Engineering from Harbin Institute of Technology (HIT), Harbin, China, in 2002, 2004, and 2009, respectively.

Since 2010, he has been an Lecturer in the School of Electrical Engineering and Automation, HIT. From June 2015 to May 2016, he was a visiting scholar at the North Carolina State University, Raleigh, USA. His current research interests include permanent magnet synchronous motor (PMSM), multi-phase PMSM, low voltage IM, sensorless control, field-weakening control.

Rui Gao (S'14) received the B.Sc. and M.Sc. degrees in electrical engineering from Harbin Institute of Technology, Harbin, China, in 2009 and 2011, respectively, and the Ph.D. degree from North Carolina State University, Raleigh, NC, USA, in 2017.

He is currently a Lead Engineer with Corporate Research and Technology Group, Eaton Corporation, Milwaukee, WI. His research interests include electric machine controls, SiC power conversion systems, and renewable energy resource integration.

Iqbal Husain (S'89–M'89–SM'99–F'09) received the Ph.D. degree in electrical engineering from Texas A&M University, College Station, TX, USA, in 1993.

In 2001, he was a Visiting Professor with Oregon State University, Corvallis, OR, USA. He is currently the Director of the NSF FREEDM Systems Center and the ABB Distinguished Professor of the Department of Electrical and Computer Engineering, North Carolina State University (NC State), Raleigh, NC, USA. He also serves as the Director of the Advanced Transportation Energy Center at NC State. He came to NC State in 2011 after serving as a Faculty Member for 17 years with The University of Akron, Akron, OH, USA, where he built a successful power electronics and motor drives program. His research interests are in advanced motor drives, electric and hybrid vehicles, and power converters and controls for distribution systems.

Dr. Husain was a Distinguished Lecturer of the IEEE Industry Applications Society (IAS) for 2012–2013. He was a recipient of the 1998 IEEE IAS Outstanding Young Member Award, the 2000 IEEE Third Millennium Medal, the 2004 College of Engineering Outstanding Researcher Award, and the 2006SAE Vincent Bendix Automotive Electronics Engineering Award. He is also the recipient of several IEEE IAS Committee prize paper awards.